COMBINED EFFECT OF PHOSPHATE AND POLYMER COATING ON CYTOTOXICITY AND HEMOCOMPATIBILITY OF IRON FOAMS

Renáta Oriňaková, Radka Gorejová, Martina Petráková, Ján Macko, Miriam Kupková, Monika Hrubovčáková, Iveta Maskaľová

Abstract

The use of resorbable metallic biomaterials for temporary implants has increased dramatically in the last decade. Degradable biomaterials are desirable in some specific pediatric, orthopedic, and cardiovascular applications, in which they may overcome the disadvantages of permanent devices. The three main biodegradable metals: Mg, Fe, and Zn, are intensively studied as temporary orthopedic implant materials. Among them, iron, and iron-based alloys, have received attention as promising materials for the temporary replacement of bones, especially for applications where strong mechanical support during the bone healing process is required. The addition of a low amount of phosphorus can improve the mechanical properties of such materials without the risk of retarding the corrosion rate or affecting cell proliferation. The main goal of this work was to study the combined effect of phosphating and polymer coating of open-cell iron foams on their cytotoxicity and hemocompatibility. Obtained results indicated the positive influence of the PEG coating layer and phosphorus addition on material cytocompatibility. Moreover, the combination of these procedures led to the inhibition of hemolysis, platelet adhesion, and thrombus formation.
Keywords: resorbable biomaterials, iron foams, cytotoxicity, hemocompatibility

INTRODUCTION

Cardiovascular diseases and musculoskeletal disorders are the most frequent health problems of human beings worldwide [1, 2]. Biomaterials are natural or artificial materials that provide innovative tools to help sustain and improve the life quality and longevity of patients [1-3]. Biomaterials are currently the focus of substantial research interest with the aim to keep up with the requirements of an aging population, and to improve the performance and safety of biomedical devices [2, 4]. A great advance has been shown in producing and designing biomaterials for tissue engineering and regenerative medicine [2, 4]. Today, several different material classes are applied in biomedicine: metals, metal alloys, polymers, ceramics, and composites [4, 5]. Metals are particularly used for load-bearing applications such as orthopedics due to their excellent mechanical properties [2, 5]. The usage of metallic materials in other applications such as vascular, coronary, and biliary stents is a common treatment as well [5, 6].

Renáta Oriňaková, Radka Gorejová, Martina Petráková, Ján Macko: Department of Physical Chemistry, Faculty of Science, P.J. Šafárik University in Košice, Slovakia
Miriam Kupková, Monika Hrubovcakova,: Institute of Materials Research, Slovak Academy of Sciences, Kosice, Slovakia,
Iveta Maskaľová: Department of Animal Nutrition, Dietetics and Animal Breeding, University of Veterinary Medicine and Pharmacy in Košice, Slovakia

At the time, permanent metallic implants with sufficient biocompatibility and fatigue strength are widely used in biomedical applications, including stainless steel, cobalt-chromium alloys, and titanium alloys [1, 2]. However, many of the implants serve their purpose in the human body during a healing process (most often 3–12 months) only and after that, the presence of the implants may induce the complications such as stress shielding, stent restenosis, chronic inflammation reactions, and prolonged physical irritation [2, 6]. The best way to overcome the mentioned limitations of permanent devices is the usage of degradable implants [2, 6, 7]. The main mission of absorbable biomaterials is to assist the healing process of diseased tissue, progressively degrade and become absorbed after fulfilling its objective, leaving no trace in the human body [7, 8]. The main advantages of biodegradable metallic materials used for temporary interventions are gradual load transfer to the healing tissue, the non-necessity of a second removal surgery, and reducing costs and patients' pain [2, 8].

Until now, magnesium, iron, zinc, and some of their alloys best match the standard requirements for biodegradable medical devices such as biocompatibility, toxicity, corrosion resistance, and maintenance of mechanical integrity [2, 5 – 7, 9].

Iron as a body-friendly and essential nutrient element in the human body is widely involved in oxygen fixation and many biochemical reactions [7, 10, 11]. Moreover, iron and its alloys exhibit good biocompatibility, hemocompatibility, anti-platelet adhesion property, and mechanical properties and hence provide adequate mechanical integrity in the long term [7, 10, 12, 13]. On the other hand, too slow degradation of iron-based materials, caused by the accumulation of corrosion products on the surface of implants, was found [7, 10 – 12, 14]. To overcome this drawback, several research attempts have been made, which include the development of new Fe-based alloy systems and composites, surface modification (such as ion implantation, and coating), and microstructural modifications [7, 12, 15-19]. Another strategy to increase the corrosion rate of iron-based biomaterials is the introduction of interconnected porosity [12, 22].

In orthopedic applications, the porous structure provides a larger surface area as compared to solid materials, enhances cell proliferation and tissue formation, allows the exchange of nutrients and metabolites, and supports the regeneration of bone and tissues [8, 12]. Furthermore, the inclusion of porosity enables to obtain of the elastic modulus adequate to that of a human bone and eliminates the stress shielding effect [23].

Porous iron-based biomaterials are commonly produced through powder metallurgy by both, the replication method using porous polyurethane templates and the space holder method using porogen material [24, 25].

In our previous papers, we demonstrated an accelerated degradation rate of iron foams with polyethylene glycol (PEG) coating as compared to uncoated iron foam owing to a decrease of local pH caused by oxidative degradation of PEG [26, 27]. Recently, the influence of the PEG layer on the degradation performance of open-cell iron and phosphorus/iron foams was elucidated [28]. In the present study, the effect of combining the phosphate coating with PEG coating on the cytotoxicity and hemocompatibility of Fe foam was investigated.

MATERIALS AND METHODS

Preparation of open-cell foams

Open-cell foams were produced through powder metallurgy by replication method. The Fe foams manufacturing process and materials used have been described in detail in our previous papers [26-28]. Briefly, the cylindrical specimens (Ø 10 mm, h 20 mm) cut from the polyurethane (PUR) foam with a pore diameter 1060–1600 μm (Filtren® TM 25133, Eurofoam, Brno, Czech Republic), were impregnated with a suspension of carbonyl iron powder (CIP) type CC d50 3.8–5.3 μm (BASF, Ludwigshafen, Germany), gelatin (Sigma-Aldrich, Saint-Louis, MO, USA) and water for 24 h. To obtain the open cell iron foams, the impregnated PUR foams were sintered in two stages, first for 2 hours at 450°C in a nitrogen atmosphere in a tube furnace Aneta 1 (ANETA, Trenčianska Teplá, Slovakia). The specimens were heated up at a rate of 1 °C/min and cooled down at a rate of 10°C/min. Then, the residual metal structures were sintered for 1 hour at 1120°C in a reduction atmosphere (90% N_2, 10% H_2). The furnace was heated up at a rate of 8°C/min and then cooled down at a rate of 10°C/min.

The same procedure was used for Fe-phosphorus (Fe/P) foams preparation, but the iron-phosphate-coated carbonyl iron powder was used as starting material and the second stage of sintering was carried out at a lower temperature (1050°C) to prevent liquid-phase sintering. The phosphate-coated iron powder was obtained by a modified precipitation process consisting of pickling the iron powder in phosphating solution (molar ratio H_3PO_4 to acetone was 9:1) at ambient temperature for 2 hours, desiccating at 60°C for 2 hours, and sintering in the air at 400°C for 3 hours. The content of phosphorus in Fe/P foam samples was about 0.5 wt.%. The microstructure and composition of phosphated CIP were reported in more detail in our previous paper [29].

Preparation of polymer-coated foams

The polymer-coated foams (Fe-PEG, Fe/P-PEG) were produced by a sol-gel process. Fe and Fe/P open cell foams were ultrasonically cleaned in acetone for 20 minutes and immersed in a 10 wt.% solution of polyethylene glycol 4000 (PEG) (Sigma-Aldrich, Saint-Louis, MO, USA) in 96% ethanol (Mikrochem spol. s.r.o., Pezinok, Slovakia) prepared in advance and kept 24 hours at room temperature. After 3 hours, the samples were taken from the solution and dried at 45°C for another 3 hours. The content of the PEG in polymer-coated foams (Fe-PEG, Fe/P-PEG), calculated from the weight differences before and after the coating layer deposition, was 3.1 - 3.3 wt.%.

Characterization of materials

The structural characterization and surface topography were revealed by a scanning electron microscope (SEM) equipped with an energy dispersive spectrometer (EDX) (JEOL JSM-7000F, Tokyo, Japan with EDX INCA).

A pore Size Analyzer (Quantachrome Instruments, HartleyWintney, UK) was applied to measure the surface area. The specific surface area (S_{BET}) of fabricated foams was determined by means of a low-temperature nitrogen adsorption method using a NOVA 1200e Surface Area and the Brunauer-Emmett-Teller (BET) theory was used to calculate the S_{BET} values.

Estimation of the theoretical sintered density (ρ) and total porosity (π) of the foam samples was performed by gravimetry. The detailed procedure for determining density and porosity has been described in previous publications [27-30]. Briefly, sintered density was determined from Archimedes' principle ((DIN ISO3369) from the following equation:

$$\rho = \frac{m_i}{\frac{m_{PA}-m_{PW}}{\rho_W} - \frac{m_{PA}-m_i}{\rho_P}} \tag{1}$$

where m_i, m_{PA}, and m_{PW} are the initial mass (g), the mass of the foam sample wrapped in Parafilm foil weighed in air (g), the mass of the foam sample wrapped in Parafilm foil weighed in water (g), ρ_W and ρ_P are the density (g cm^{-3}) of water and Parafilm.

The total porosity of foam specimens was calculated using the following equation [30]:

$$\pi = \left(1 - \frac{m_i}{(m_{BA}-m_{BW}) \cdot \rho}\right) \times 100\% \tag{2}$$

where m_i, m_{BA}, and m_{BW} are the initial mass (g), the mass of the benzyl alcohol-soaked foam weighed in air (g), the mass of the benzyl alcohol-soaked foam weighed in water (g), ρ is the theoretical density of foam (g cm^{-3}).

Cell viability testing
Extract preparation

UV-disinfected foam samples (Fe, Fe/P, Fe-PEG, Fe/P-PEG) and stainless steel (SS) sheet (10 x 20 x 0.7 mm^3, STN 17246) as control were separately immersed into a sterile polypropylene centrifuge tubes containing complete culture medium composed of Dulbecco's Modified Eagle's Medium (DMEM) with 10% fetal bovine serum (FBS) and 1% antibiotic solution (all from Merck KGaA, Darmstadt, Germany) (1 ml/10 cm^2 of the sample surface area) at 37 °C for 24 hours. After 24 hours of immersion, all samples were removed and the medium was centrifuged (10,000 rpm, 10 minutes) to collect extracts free of sample residues which were used for further testing. Extracts were further diluted to 100%, 50%, and 10% with a complete culture medium to test extract concentration dependence on cell viability.

Cytotoxicity testing

The cell toxicity testing was performed according to STN ISO 10993-5 norm [31]. To culture semi-confluent monolayers of cells, 1×10^4 of adult human dermal fibroblast (HDFa) cells (Merck KGaA, Darmstadt, Germany) were suspended in 100 ml of complete culture medium and seeded into 96-well cell microplate and were incubated at 37° C in 95% humidity and 5% CO$_2$ for 24 hours. After 24 hours of incubation, the culture medium from each well was removed and wells were rinsed with phosphate-buffered saline (PBS) (w/calcium, w/magnesium, Sterile Filtered, Biowest, Nuaillé, France). Subsequently, 100 μl of 100%, 50%, and 10% extracts prepared as described above were added to the wells with seeded cells and were left for incubation for 4, 24, or 72 hours. All experiments were carried out in triplicate and 100 μl of fresh complete culture medium was used as negative control (NC). The cytotoxic effect of the extract was evaluated by the MTS proliferation test assay (Cell titer 96 aqueous one solution cell proliferation assay, Promega, USA). The absorbance of formazan produced by the mitochondrial enzyme activity after 4, 24, or 72 hours of cultivation was measured (ELISA microplate reader, UT-2100C, MRC Lab, Israel) Cytotoxicity was expressed as a percentage relative to the negative control (set as 100% viability).

Hemocompatibility testing

A healthy cow's blood was taken for testing. Sodium citrate (with 3.8 wt.%, in the ratio of 9:1) was added to the blood collection tubes as an anticoagulant. Blood containing sodium citrate (3.8 wt.%) was diluted in a ratio of 1:10 with saline solution for further use.

Hemolysis test

The prepared sterilized metallic foam samples were placed in test tubes, and 5 ml of physiological saline was added to each sample. The samples were incubated at 37 °C for 30 min. Positive and negative controls were prepared into separate tubes according to the following procedures. Positive control (PC) corresponding to the complete hemolysis of red blood cells (RBCs) was consisting of 5 ml of 0.1% Na_2CO_3 solution and 0.1 ml of diluted blood. Negative control (NC) was prepared by mixing 5 ml saline and 0.1 ml diluted blood. Subsequently, 0.1 ml of diluted blood was added to each tube with the sample, and incubation was continued for 60 min. After incubation, samples were taken from the solutions and the tubes were centrifuged for 5 minutes at 3000 rpm. The supernatant was carefully transferred to a spectrometric cuvette and the absorbance at 540 nm was measured (Biochrom WPA Lightwave II UV/Visible Spectrophotometer, Biochrom Ltd, Cambridge, United Kingdom). The hemolysis ratio (H) was calculated using equation (3):

$$H(\%) = \frac{OD - OD_{NC}}{OD_{PC} - OD_{NC}} \cdot 100\%$$ (3)

where OD, ODNC, and ODPC are the mean optical densities of the tested foams, negative control, and positive control, respectively.

Thrombus formation test

Sterilized and weighed foam samples were placed in tubes containing 1 ml of PBS. The sample tubes were incubated at 37 °C for 30 minutes. Then, 0.1 ml of diluted blood was applied onto the surface of the samples and 0.1 ml of 0.1 M $CaCl_2$ was subsequently added dropwise to initiate the formation of clots. After 30 minutes, the samples were rinsed with distilled water to stop the coagulation reaction. The formed blood clots were separated, immersed in distilled water for 5 minutes, and fixed in formaldehyde for 10 minutes. The precipitates were dried to constant weight and weighed.

Platelet adhesion test

The prepared foam samples were incubated in PBS for 30 minutes at 37 °C. Platelet-rich plasma (PRP) was prepared by centrifuging the undiluted blood for 15 minutes at 1600 rpm. After incubation, samples were removed from the buffer and immersed in 1 ml of prepared blood plasma at 37 °C for 2 h. The samples were then rinsed with PBS to remove non-adherent platelets. A series of ethanol/distilled water solutions were prepared in concentrations from 50/50 to 100/0% in 10% increments. In each of these solutions, the samples were dehydrated at 4 °C for 10 minutes. After dehydration, samples were lyophilized for 2 days and subsequently monitored by SEM (JEOL JSM-7000F with EDX INCA, Japan).

EXPERIMENTAL RESULTS AND DISCUSSION

Open cell iron-based foams with porosity of 84%, 80%, 89%, and 87%, for Fe, Fe/P, Fe-PEG, and Fe/P-PEG samples, corresponding to a density of 0.73 ± 0.05 g cm^{-3}, 0.80 ± 0.02 g cm^{-3}, 0.89 ± 0.04 g cm^{-3}, and 0.87 ± 0.04 g cm^{-3}, respectively, were manufactured by powder metallurgy method and subsequent polymer coating.

Surface morphology and composition

Fig. 1 shows the SEM micrographs of the iron-based foams at two different magnifications and the chemical composition of the surface determined from EDX analysis. From the morphological characterization, it was found that the structure of the sintered iron and phosphated iron samples are similar to that of open-pore polyurethane foam used in the fabrication process (Figs. 1a-d). Produced foams possessed interconnected porosity which included macroporosity in the range of 400 μm to 1500 μm and random spherical microporosities in the strut (under 5 μm). Nodular surface morphology resulted from the sintering of powder particles (Figs. 1e, 1g). Foams manufactured from phosphated iron powder (Fig. 1c) exhibited slightly higher pore size as compared to iron foams (Fig. 1a). General appearance of foams with polymer layer (Figs. 1b, 1d) coincides with a macroscopic view with that of un-coated foams (Figs. 1a, 1c). However, SEM micrographs taken at higher magnification demonstrated a much smoother and more even surface of polymer-coated foams (Figs. 1f, 1h) due to the polymer filling of the pores. In some places, uncovered iron tops protrude above the polymer layer. This was also confirmed by EDX analysis of the chemical composition of the surface of foam samples (Fig. 1). The iron content on the surface areas with protruding iron nodules is higher than on smooth surface areas indicated in Figs. 1f and 1h. The presence of carbon and oxygen in the surface composition is another confirmation of PEG layer deposition onto the foam specimens' surface. The phosphorus content on the surface was below the limit of reliable determination. The lower porosity and surface roughness of the polymer-coated samples was also associated with a smaller specific surface area, which was 0.48 $m^2 g^{-1}$, 0.50 $m^2 g^{-1}$, 0.44 $m^2 g^{-1}$, and 0.45 $m^2 g^{-1}$ for Fe, Fe/P, Fe-PEG, and Fe/P-PEG samples, respectively.
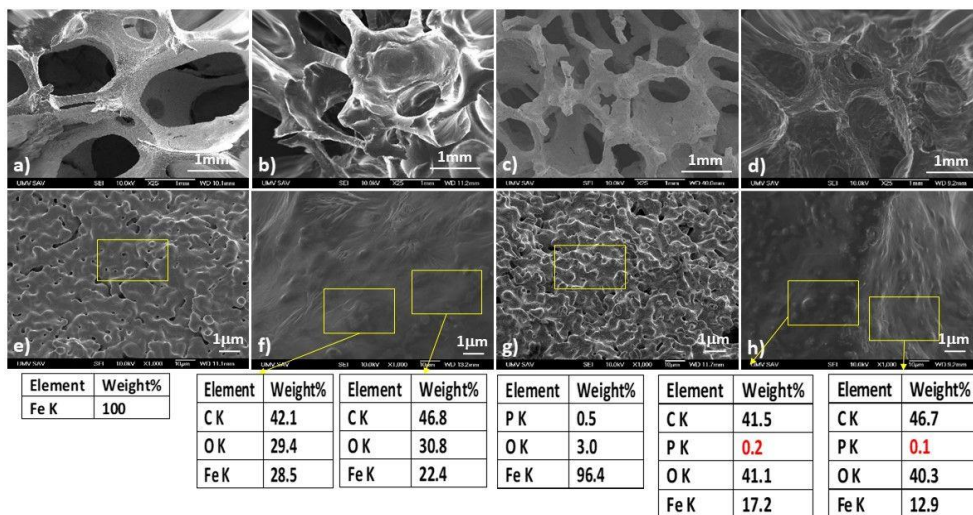

Fig. 1. SEM micrographs of the surface of iron-based foams: Fe (a, e); Fe-PEG (b, f); Fe/P c, g); and Fe/P-PEG (d, h) and chemical composition of their surface determined from EDX analysis. Magnification: 25× (a, b, c, d); 1000× (e, f, g, h).

Cell viability

The MTS test was employed to assess the cytotoxicity of foam samples intended for potential orthopedic application. Fig. 2 shows the viability of HDFa cells cultured in extraction medium (100%, 50%, and 10%) for 4, 24, and 72 hours (Fig. 2 a-c) and values of pH of the obtained undiluted extracts (Fig. 2d). Relative cell viability expressed as a relative to the cell viability obtained for negative control decreased with increasing incubation time for all experimental samples. The viabilities of cells incubated with uncoated foams extraction mediums were slightly lower than those cultured with PEG-coated foams extracts. Compared to iron samples, the phosphating of CIP exhibited a positive effect on the viability of HDFa cells.

After 4 hours of incubation, all studied samples showed high cytocompatibility even for undiluted extracts (between 80 and 94 %). With the increase of incubation time, the cell viabilities started to decline and after 24 hours, only cells cultured in extracts obtained from the Fe/P-PEG sample were maintaining values of relative cell viability above 80 % among undiluted specimen extracts (Figs. 2a-c). After 72 hours of incubation with extracts, the viabilities of cells for all the foam samples decreased under 70 % and the differences in cell viability for the extracts of the modified samples were insignificant. The positive effect of extract dilution on the relative cell viability was observed, however, no significant increase in cell viability was spotted.
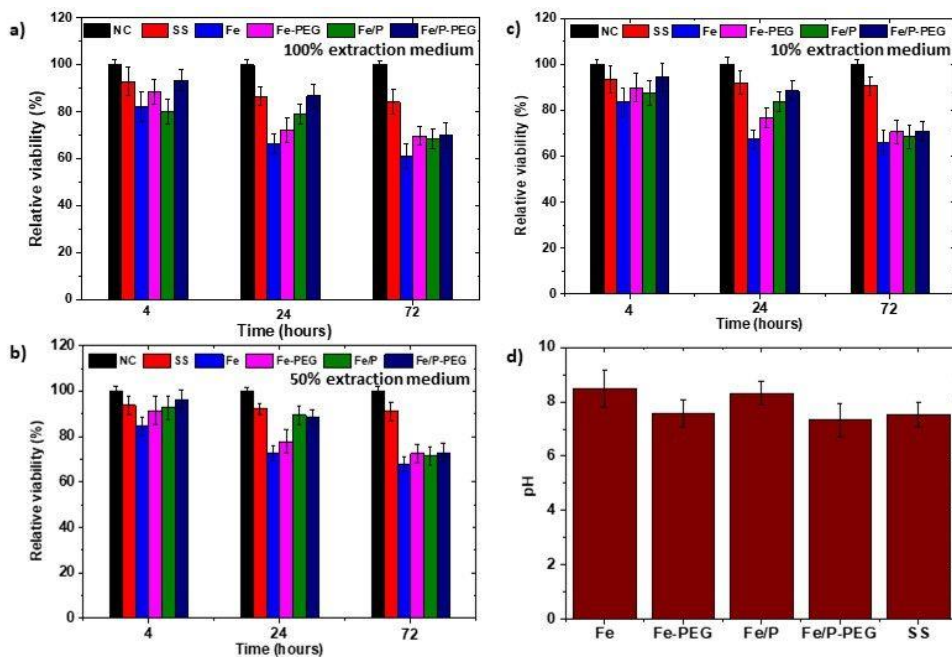

Fig. 2. Relative viability of HDFa cells obtained from MTS assay after cultured for 4, 24, and 72 hours (a-c) in extraction mediums of Fe, Fe-PEG, Fe/P, Fe/P-PEG foams, stainless steel sheet, and negative control: 100% (a), 50% (b), 10% (c), and pH of undiluted sample´s extracts (d).

In general, coated samples showed better biocompatibility than un-coated samples and among them, Fe/P-PEG exhibited higher relative cell viability than Fe-PEG. The positive effect of PEG coating on biocompatibility could be associated with the release of protons due to the oxidative degradation of the polymer layer [8, 26, 28, 32] which allow the compensation of pH increase owing to corrosion of iron scaffolds during immersion in the cultivation medium. This resulted in a lower rise in the pH value of the culture medium during extracts preparation, as follows from Fig. 2d.

Hemocompatibility

Results of *in vitro* hemocompatibility testing are illustrated in Fig. 3. Fig. 3a shows the calculated hemolysis percentage values for iron-based foam samples, which were all below 10%, so the fabricated foams can be considered as hemocompatible. Except for bare iron foam, the hemolysis values were even lower than 5%, indicating good hemocompatibility of foam materials.
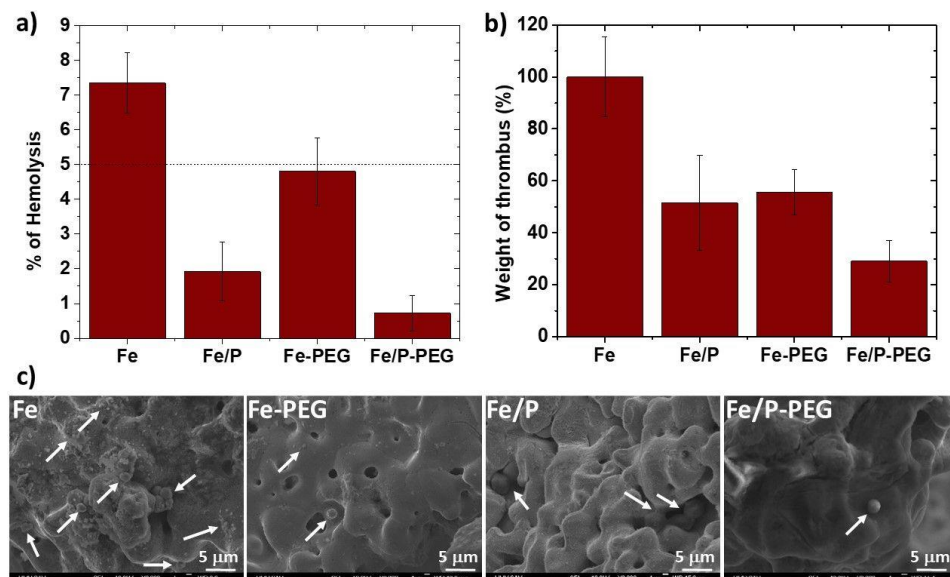

Fig. 3. Percentage of hemolysis induced by fabricated foams (a), percentage weight of blood clots formed on foam samples (b), and SEM micrographs of platelets adhering to the surface of iron-based foams (c).

Testing of coagulation induced by fabricated foams was performed by a weighting of thrombus formed on samples in contact with blood. Fig. 3b reveals the percentage of the weight of blood clots precipitated on the experimental samples compared to thrombus weight formed on uncoated Fe foam as standard (100 %). The blood clotting was about 50% lower on iron phosphate (Fe/P) and polymer-coated iron foam (Fe-PEG) when compared to bare iron foam. An even more pronounced decrease in thrombus weight was observed for the Fe/P-PEG foam with a reduction in thrombus weight percentage of about 70%, indicating minimum blood clotting.

Adsorption of platelets is one of the key steps of blood clot formation. The amount and morphology of platelets adhered to the surface of fabricated foam specimens were examined by SEM (Fig. 3c). Activated platelets which started to form dendrites, and aggregate was detected on the surface of bare iron foam together with the highest number of adherent platelets. A lower amount of adhering platelets with spherical morphology was observed on Fe/P and Fe-PEG foams. Only a few platelets adhered on the surface of Fe/P-PEG foam. In accordance with the results of antithrombotic activity, it can be concluded that the phosphating and polymer coating resulted in the elimination of platelet adsorption.

CONCLUSIONS

In summary, iron-based foams have been fabricated using a powder metallurgy technique. With the aim to tailor the biocompatibility of iron biomaterials, the effect of phosphating in combination with PEG coating on the *in vitro* cytotoxicity and hemocompatibility of iron foams was evaluated in this work.

The indirect cytotoxicity test results indicate the positive effect of surface modification by PEG coating and phosphating. However, after 72 hours of incubation with extracts, the viability of cells dropped below 70% and was approximately the same for all modified foams. With the exception of bare iron foam, the hemolysis was below 5%, exhibiting its slightly damaging effect on erythrocytes. The antithrombotic activity of modified foams was significantly higher when compared to bare iron foam. The positive effect of the combination of phosphating and PEG coating was also confirmed by the suppression of platelet adsorption.

Based on the results obtained, it can be concluded that modification of the surface of iron foams by the combination of phosphating and polymer coating represents a useful approach toward the development of degradable iron-based foam materials for potential orthopedic applications.

ACKNOWLEDGMENT

REFERENCES

[1] Santos, C., Alves, MM., Montemor, MF., Carmezim, MJ.: Bioresorbable metallic implants: surface functionalization with nanoparticles and nanostructures, in: I. Ahmad, P. Di Sia, R. Raza (Eds.), Advanced Materials and their Applications: Micro to nano scale, One Central Press, 2017, p. 219.

[2] dos Santos, GA.: Adv. Tissue Eng. Regen. Med., vol. 3, 2017, p. 300.

[3] Victor, SP., Selvam, S., Sharma, CP.: ACS Biomater. Sci. Eng., vol. 5, 2019, p. 3.

[4] Hinderer, S., Brauchle, E., Schenke-Layland, K.: Adv. Healthcare Mater., vol. 4, 2015, p. 2326.

[5] Allain, JP., Echeverry-Rendón, M.: Surface treatment of metallic biomaterials in contact with blood to enhance hemocompatibility, in: C.A. Siedlecki (ed.), Hemocompatibility of Biomaterials for Clinical Applications. Blood-Biomaterials Interactions, Elsevier Ltd., Woodhead Publishing, 2018, p. 279.

[6] Jurgeleit, T., Quandt, E., Zamponi, C.: Adv. Mater. Sci. Eng., vol. 2015, 2015, p. 294686.

[7] Adhilakshmi, A., Ravichandran, K., Sankara Narayanan, TSN.: New J. Chem., vol. 42, 2018, p. 18458.

[8] Yusop, AH., Daud, NM., Nur, H., Kadir, MR., Hermawan, H.: Sci. Rep., vol. 5, 2015, p. 11194.

[9] Lia, H., Zhenga, Y., Qin, L.: Prog. Nat. Sci.: Mater. Int., vol. 24, 2014, p. 414.

[10] Huang, T., Zheng, Y.: Sci. Rep., vol. 6, 2016, p. 23627.

[11] Nie, FL., Zheng, YF., Wei, SC., Hu, C., Yang, G.: Biomed. Mater., vol. 5, 2010, p. 065015.

[12] Sharma, P., Gopal Jain, K., Pandey, PM., Mohanty, S.: Mater. Sci. Eng. C, vol. 106, 2020, p. 110247.

[13] Dehestani, M., Adolfsson, E., Stanciu, LA.: Mater. Des., vol. 109, 2016, p. 556.

[14] Huang, T., Zheng, Y., Han, Y.: Regen. Biomater., vol. 3, 2016, p. 205.

[15] Heiden, M., Walker, E., Nauman, E., Stanciu, L.: J. Biomed. Mater. Res. A, vol. 103, 015, p. 185.

[16] Čapek, J., Msallamová, Š., Jablonská, E., Lipov, J., Vojtěch, D.: Mater. Sci. Eng., C, vol. 79, 2017, p. 550.

[17] Wang, H., Zheng, Y., Jiang, Ch., Li, Y., Fu, Y.: Surf. Coat. Technol., vol. 320, 2017, p. 201.

[18] Lee, MK., Lee, H., Park, Ch., Kang, IG., Kim, J., Kim, HE., Jung, HD., Jang, TS.: Bioact. Mater., vol. 9, 2022, p. 239.

[19] Qi, Y., Qi, H., He, Y., Lin, W., Li, P., Qin, L., Hu, Y., Chen, L., Liu, Q., Sun, H., Liu, Q., Zhang, G., Cui, S., Hu, J., Yu, L., Zhang, D., Ding, J.: ACS Appl. Mater. Interfaces, vol. 10, 2018, p. 182.

[20] Gąsior, G., Szczepański, J., Radtke, A.: Materials, vol. 14, 2021, p. 3381.

[21] Li, Y., Jahr, H., Lietaert, K., Pavanram, P., Yilmaz, A., Fockaert, LI., Leeflang, MA., Pouran, B., Gonzalez-Garcia, Y., Weinans, H., Mol, JMC., Zhou, J., Zadpoor, AA.: Acta Biomater., vol. 77, 2018, p. 380.

[22] Putra, NE., Leeflang, MA., Minneboo, M., Taheri, P., Fratila-Apachitei, LE., Mol, JMC., Zhou, J., Zadpoor, AA.: Acta Biomater., vol.121, 2021, p. 741.

[23] Wegener, B., Sichler, A., Milz, S., Sprecher, C., Pieper, K., Hermanns, W., Jansson, V., Nies, B., Kieback, B., Müller, P.E., Wegener, V., Quadbeck, P.: Sci Rep., vol. 10, 2020, p. 9141.

[24] Ray, S., Thormann, U., Eichelroth, M., Budak, M., Biehl, C., Rupp, M., Sommer, U., El Khassawna, T., Alagboso, F.I., Kampschulte, M., Rohnke, M., Henß, A., Peppler, K., Linke, V., Quadbeck, P., Voigt, A., Stenger, F., Karl, D., Schnettler, R., Heiss, C., Lips, K.S., Alt, V.: Biomaterials, vol. 157, 2018, p. 1.

[25] Quadbeck, P., Stephani, G., Kümmel, K., Adler, J., Standke, G.: Mater. Sci. Forum, vol. 534-536, 2007, p. 1005.

[26] Haverová, L., Oriňaková, R., Oriňak, A., Gorejová, R., Baláž, M., Vanýsek, P., Kupková, M., Hrubovčáková, M., Mudroň, P., Radoňák, J., Orságová Králová, Z., Morovská Turoňová, A.: Metals, vol. 8, 2018, p. 499.

[27] Oriňaková, R., Gorejová, R., Orságová Králová, Z., Haverová, L., Oriňak, A., Maskaľová, I., Kupková, M., Džupon, M., Baláž, M., Hrubovčáková, M., Sopčák, T., Zubrik, A., Oriňak, M.: App. Surf. Sci., vol. 505, 2020, p. 144634.

[28] Oriňaková, R., Gorejová, R., Petráková, M., Orságová Králová, Z., Oriňak, A., Kupková, M., Hrubovčáková, M., Podobová, M., Baláž, M., Smith, R.M.: Materials, vol. 13, 2020, p. 4134.

[29] Orinakova, R., Orinak, A., Giretova, M., Medvecky, L., Kupkova, M., Hrubovcakova, M., Maskalova, I., Macko, J., Kalavsky, F.: J. Biomater. Appl., vol. 30, 2016, p. 1060.

[30] Hrubovčáková, M., Kupková, M., Džupon, M.: Adv. Mater. Sci. Eng., vol. 2016, 2016, p. 6257368.

[31] ISO-10993–5. Biological evaluation of medical devices—part 5 tests for cytotoxicity: in vitro methods. Arlington: ANSI/AAMI; 2009.
[32] Oriňaková, R., Gorejová, R., Macko, J., Oriňak, A., Kupková, M., Hrubovčáková, M., Ševc, J., Smith, R.M.: Appl. Surf. Sci., vol. 475, 2019, p. 515.

EFFECT OF SINTERING TIME ON MECHANICAL PROPERTIES OF (Hf-Ta-Zr-Nb-Ti)C

Lenka Dakova, Monika Hrubovcakova, Richard Sedlak, Alexandra Kovalcikova, Lubomir Medvecky, Annamaria Naughton-Duszova, Iveta Vaskova, Jan Dusza

Abstract

Advanced high-entropy (Hf-Ta-Zr-Nb-Ti)C ceramics were successfully fabricated by the combination of ball milling and a two-step sintering process at 2100 °C for 5, 10, and 20 minutes from commercially available powders. The microstructure characteristics and mechanical properties of the developed systems were investigated. The high-entropy ceramics exhibit: medium grain size from 8 μm to 11 μm, high compositional uniformity, and high relative density above 99.5 %. Vickers hardness for all systems decreased with increasing applied load, with the highest value HV1 = 22.0 GPa for the system sintered for 5 minutes, while the fracture toughness changed from 2.70 MPa.m$^{1/2}$ to 3.50 MPa.m$^{1/2}$. The highest four-point flexural strength of 284 MPa was measured for the system with the smallest grain size.

Keywords: high-entropy carbide, spark plasma sintering, XRD analysis, Vickers hardness, indentation fracture resistance, bending strength

INTRODUCTION

During the last years, the field of high entropy ceramics has attracted significant research interest, stimulated by the discoveries on high entropy alloys (HEAs). HEAs with a highly disordered and homogeneous chemical composition and a single crystalline phase have been reported to have remarkable mechanical properties, wear, corrosion resistance, etc. [1-2].

Bulk high-entropy ceramics are a new group of advanced ceramics, consisting of at least four different metallic elements stabilized by the configurational entropy, developed mainly as potential structural materials for extreme environment applications [3,4]. Bulk single-phase high-entropy carbides have been synthesized for the first time in 2018, with the aim to develop structural materials, which broaden the limited set of ultra-high temperature ceramics [5].

The research of high-entropy carbides during the last years focused on several main directions: theoretical calculations, development, and application of new processing routes, microstructure characterization, testing of mechanical properties at nano/micro/macro level, and testing of the oxidation, creep and wear characteristics [3-7].

Yan et al. [8] reported low thermal conductivity and diffusivity of the five-component high-entropy carbide $(Hf_{0.2}Zr_{0.2}Ta_{0.2}Nb_{0.2}Ti_{0.2})C$. The low thermal conductivity is associated with severe phonon scattering, which is induced by the lattice distortion in the multicomponent rock salt structure.

Lenka Dakova, Monika Hrubovcakova, Richard Sedlak, Alexandra Kovalcikova, Lubomir Medvecky, Annamaria Naughton-Duszova, Jan Dusza: Institute of Materials Research, Slovak Academy of Science, Kosice, Slovakia,
Iveta Vaskova: Technical University of Kosice, Faculty of Materials, Metallurgy, and Recycling, Institute of Materials, Kosice, Slovakia
Ján Dusza: Donát Bánki Faculty of Mechanical and Safety Engineering, Óbuda University, Budapest, Hungary

Feng et. al. [9] produced carbide powders of (HfZrTiTaNb)C with relative density upper than 95% with grain size from 0.6 um to 1.2 um by hot pressing. Young's modulus increased from 405 ± 10 GPa to 452 ± 6 GPa and Vickers hardness measured under a load of 4.9 N increased from 23.7 ± 0.3 GPa to 24.8 ± 0.8 GPa as the densification temperature increased from 1750 °C to 1900 °C.

Moskovskikh et al. [10] fabricated (HfTaTiNbZr)C and (HfTaTiNbMo)C systems through the reactive high-energy ball milling of metal and graphite particles. The (HfTaTiNbZr)C ceramic possess a relative density of up to 94.8%, hardness of 25.7 ± 3.5 GPa, and Young's modulus of 473 ± 37 GPa. (HfTaTiNbMo)C ceramics with a relative density of up to 93.8%, hardness of 23.8 ± 2.7 GPa, and Young's modulus of 544 ± 48 GPa.

Dusza et al. [11] developed (Hf-Zr-Ta-Nb-Ti)C high entropy carbide with high relative density and single phase high entropy grains by ball milling of commercially available carbide powders and two-step sintering. The system shows high hardness and good tribological properties with a dominant wear mechanism in the form of mechanical wear, with limited grain pull-out and fracture, and with localized tribolayer formation.

The aim of the present contribution is to study the influence of the processing methods on the microstructure development and Vickers hardness, indentation fracture resistance, and bending strength of high-entropic carbide (Hf-Ta-Zr-Nb-Ti)C.

EXPERIMENTAL MATERIALS AND METHODS

The commercially available raw powders used in this study include TiC (99.5 %, typically ~ 2 µm, Alfa Aesar), ZrC (99.5 %, ~ 44 µm, Alfa Aesar), HfC (99.5 %, ~ 44 µm, Alfa Aesar), NbC (99 %, < 10 µm, Alfa Aesar), and TaC (99.5 % purity, < 44 µm, Alfa Aesar). The raw powders were mixed in an equal molar ratio: 0.20 mol.% TiC, 0.20 mol.% ZrC, 0.20 mol.% HfC, 0.20 mol.% NbC, 0.20 mol.% TaC, and homogenized/milled using a planetary ball mill in a polyethylene-lined jar with tungsten carbide balls as milling media. The ball milling was performed for 4 h at a speed of 250 rpm in argon to reduce the contamination with oxygen. The ball-milled powder mixture was then transferred into a graphite die with a diameter of 20 mm and spark plasma sintered by a two-step sintering process. Afterward, the sample was heated in a vacuum to 1800 °C at a heating rate of 100 °C/min and held for 10 min. Then, argon was introduced into the chamber, and the pressure was continuously increased to 70 MPa while increasing the temperature up to the maximum of 2100 °C at a 50 °C/min heating rate. The samples were sintered at 2100 °C for 5, 10, and 20 minutes, respectively as System I, II, and III, respectively. The final samples were cooled to room temperature at a rate of 100 °C/min.

The density of the prepared systems was measured by Archimedes' principle using distilled water as an immersion liquid and held for 4 h in a vacuum.

Due to the high hardness and durability of the inner ceramic materials, the methodology of preparation for the observation of microstructures required the use of diamond tools. The whole process of preparing ceramographic systems involved grinding and polishing. Grinding was performed on grinding wheels with diamond abrasives of various grain sizes (from 15 µm to 1 µm). After successful grinding, the specimens were finely polished and etched using a submicron colloidal silica suspension for 5 minutes to eliminate the slightest surface defects and reveal the structure. To remove the impurities that came from the polishing wheel the specimens were immersed in ethanol and sonicated for 4 minutes. This step removed all residual impurities in the systems.

Morphologies and microstructure were characterized by scanning electron microscopy (FIB-SEM ZEISS AURIGA Compact). The crystal structure of the powders

was characterized by X-ray diffraction. Philips X'Pert Pro laboratory X-ray in a Bragg-Brentano arrangement was used to characterize the powder. The measurements were performed in the 2Θ range from 30° to 80°. The Vickers hardness measurements were carried out under different applied loads of 9.81 N (1kg), 29.43 N (3kg), and 49.03 N (5kg), respectively, with a holding time of 10 s on the polished surfaces. For each applied load 8 imprints were made. The test consisted of pressing a diamond regular quadrilateral pyramid with a top wall angle of 136 ° into the examined systems. To determine the hardness, the individual diagonals of the impressions were measured. Vickers hardness values were determined according to Equation (1):

$$HV = 0{,}189 \cdot \left(\frac{P}{d^2}\right)$$

where P is the applied load (N), and d is the arithmetic mean of the length of the diagonals of the indentation.

The indentation method was used to measure the fracture toughness by using the Vickers hardness tester, and Equation (2), valid for semi-circular crack systems as proposed by Anstis et al. [12] for calculation is as follows:

$$K_{IC} = 0{,}016 \left(\frac{E}{H}\right)^{1/2} \frac{P}{c^{3/2}}$$

where 0.016 is the material-independent constant for Vickers-produced radial cracks, E is Young's modulus (GPa), H is Vicker's hardness (GPa), P is the applied load (N), and c is the length of the radial crack (μm).

The flexural strength test for investigated systems was performed according to ASTM C1161-13 [13]. The system was tested in a four-point bending setup (inner support span 8 mm and outer support span 16 mm) with a feed rate of 0.5 mm/min at ambient temperature. From the measured values of the force at which the system broke, the values of the four-point flexural strength were calculated according to Equation (3). Each specimen was cut with a diamond saw to measure flexural strength and static modulus of elasticity. All cut patterns of approximately 2×3×25 mm were ground using diamond wheels with a grain size from 15 μm to 1 μm and then polished with polycrystalline diamond paste. The two edges on the system surface were trimmed at a 45 ° angle to eliminate defects initiated from the system edge. The four-point flexural strength was calculated according to the relation (3):

$$\sigma_{OH} = \frac{3P(S_1 - S_2)}{2BW^2}$$

where P is the load, measured at the moment of the fracture (N), S_1 is outer span distance (mm), S_2 is inner span distance (mm), B is the width of the system (mm), W is the height of the system (mm).

RESULTS AND DISCUSSION

The results illustrated in Tab. 1 show that the densification process was very good, and the processed systems are with very high relative density from 99.54 to 99.9 %. Fig. 1 shows the XRD patterns of the individual binary carbides used in the present work, along with the patterns of the as-sintered material for the system sintered for 5 minutes. The lattice parameter for System I, which was sintered for 5 minutes, was 4.514 A ± 2.46 E^{-5}. Increased holding time did not affect the lattice parameters. The parameters for the remaining systems were the same. These results confirmed that a single-phase solid solution $(Hf_{0.2}Zr_{0.2}Ta_{0.2}Nb_{0.2}Ti_{0.2})C$ with the same rock-salt structure as those of binary

metal carbides was formed during sintering. No unreacted binary carbides or oxide impurities from initial powders were identified in the final sintered system. The results for the systems sintered at 10 and 20 minutes are very similar.

Tab. 1. Density and grain size of the investigated systems

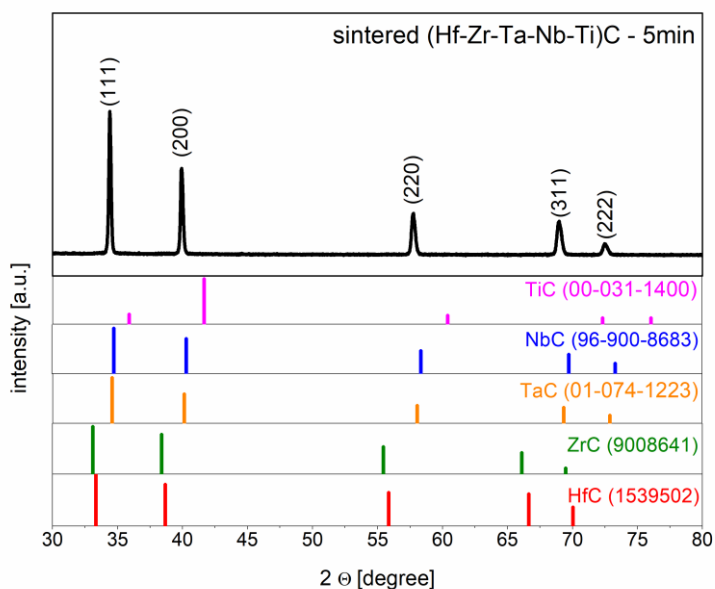|	Sintering time (min)	Theoretical density (g.cm^{-3})	Bulk density (g.cm^{-3})	Relative density (%)	Average grain size (μm)
System I	5	9.39	9.35	99.61	8.1
System II	10	9.39	9.34	99.54	8.4
System III	20	9.39	9.39	99.9	11

Fig. 1. XRD pattern of the System I sintered 5 minutes

In Fig. 2 individual SEM micrographs are illustrated with matching EDS maps of the System I prepared by SPS at 2100 °C for 5 minutes. A very small number of pores and crack-like pores at grain boundaries are present on the polished surface of this system, similarly as for all studied materials, which may originate from incomplete densification or polishing effect. The grain size of this system is changing from 4 to 15 μm with an average grain size of 8.1 μm. The average grain size for the system sintered at 10 min is similar with the value of 8.4 μm, while the average grain size of the ceramic sintered at 20 min is 11.0 μm. That's why the increased sintering time increased the grain size of the systems.

From EDS elemental mappings it is evident, five metallic components Ti, Zr, Hf, Nb, and Ta exhibit a homogeneous distribution without any elemental segregation at the microscale level. These five different elements show an almost equimolar ratio, indicating that the distribution of each element is homogeneous within the investigated systems. As an example, System I along with the respective EDS map is shown below (Fig. 2). The

elemental composition of the selected point, marked by a red cross in Fig. 2a, and a statistical chart of grain size distribution are depicted in Figs. 2b and c, respectively.
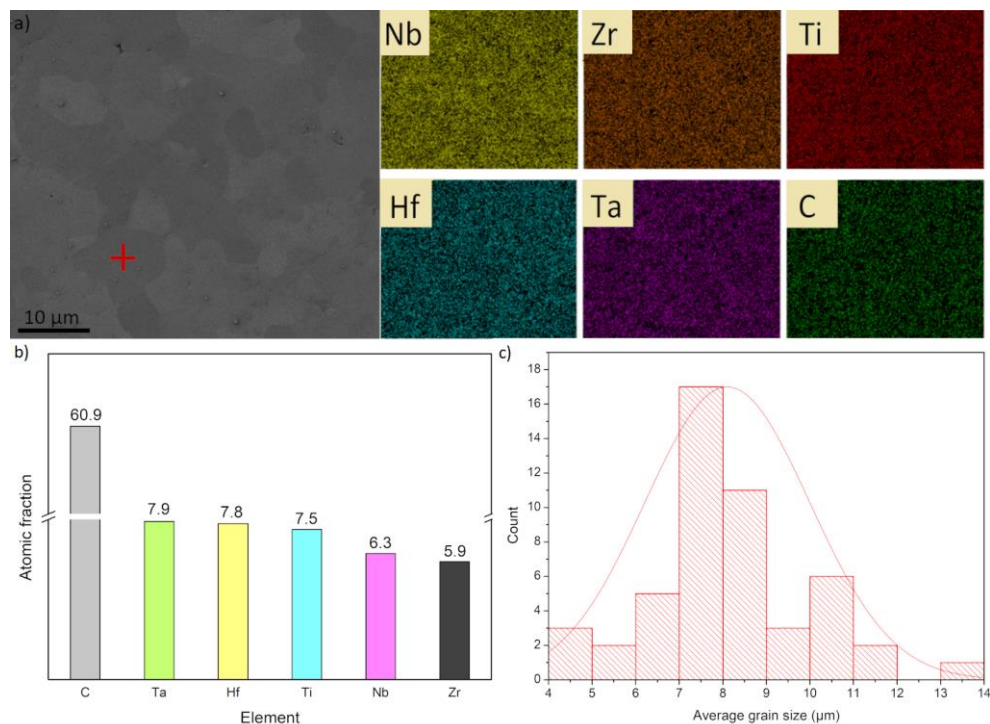

Fig. 2. SEM image of the polished surface with the corresponding EDS maps; b) the elemental composition of point as marked as a red cross in (a), and c) grain size distribution for System I (sintered for 5 minutes).

The Vickers hardness and fracture toughness of (Hf-Ta-Zr-Nb-Ti)C ceramics are listed in Tab. 2. According to the results, the influence of the sintering time and indentation load on measured hardness values is not significant, with the hardness values changing from 18.9 to 22.0 GPa. For standard HV1 Vickers hardness, the values change from 20.2 to 22.0 GPa, with the highest value obtained for the system with the largest average grain size. This can be connected with the lower porosity in the case of this system.

According to Equation (2) for the examined System I, the fracture toughness increased at a load of 29.43 N, but with increasing indentation load, the fracture toughness decreased slightly. In the case of System II, we found a decrease in the value at an indentation load of 49.03 N. The highest value in System III was recorded at an indentation load of 49.03 N. The relatively low values of fracture toughness for the investigated systems can be explained by the low number of toughening mechanisms arising during the crack propagation in the form of crack deflection, crack branching and crack bridging.

Tab. 2 Vickers hardness and fracture toughness of studied materials

	HV1 (GPa)	HV3 (GPa)	HV5 (GPa)
System I	20.9±2.4	20.1±1.5	20.7±1.9
System II	20.2±0.8	19.4±0.5	20.5±1.0
System III	22.0±1.6	19.3±1.1	18.9±1.1
	K_{IC} (MPa.m$^{1/2}$)	K_{IC} (MPa.m$^{1/2}$)	K_{IC} (MPa.m$^{1/2}$)
System I	2.9±0.3	3.1±0.4	3.0±0.1
System II	2.9±0.3	3.0±0.2	2.8±0.3
System III	2.8±0.4	3.2±0.7	3.5±0.3

The influence of different sintering times on the bending strength of the investigated materials is shown in Fig. 3. The results showed that the system that was sintered for 5 minutes reached the highest bending strength value of 284.04±13.74 MPa and the force at which the system broke was 378.93 N. In the case of System II, the breaking value slightly decreased to 225.22 N, and the value in bending values of 210.13±23.39 MPa. As for Systems III, which was sintered for 20 minutes, the breaking force was recorded as 195.99 N, while the bending strength value was 148.01±19.15 MPa. The stated decrease in strength values is closely related to the microstructure of the given materials, where grain growth occurs with increasing sintering time.
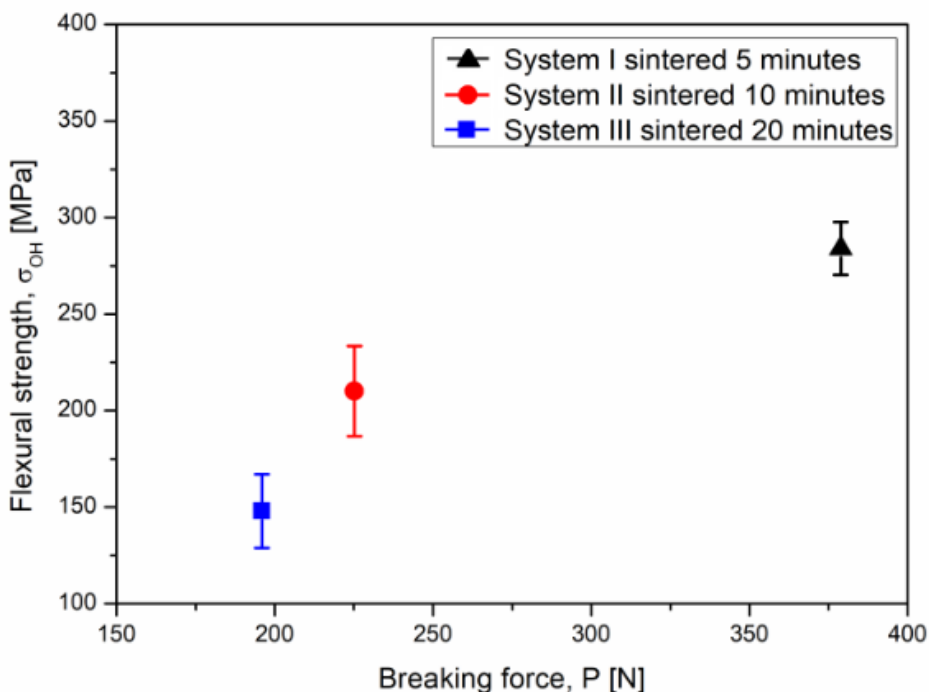

Fig. 3. Bending strength of the studied materials

After the four-point bending strength test, the broken samples were subjected to fractographic analysis in order to determine the initiation point of the fracture. The fractographic analysis showed that intergranular failure occurs on the fracture surface of all investigated materials. Carbon agglomerates were also found on the tensile surface. Fractographic analyses revealed that the strength degrading defects are connected crack–like pores located at the grain boundaries, very close to the tensile surface of the tested bending bar. Characteristic fracture surfaces of the studied systems I and III are shown in Fig. 4. As it is visible the fracture mode is mixed inter and transgranular.
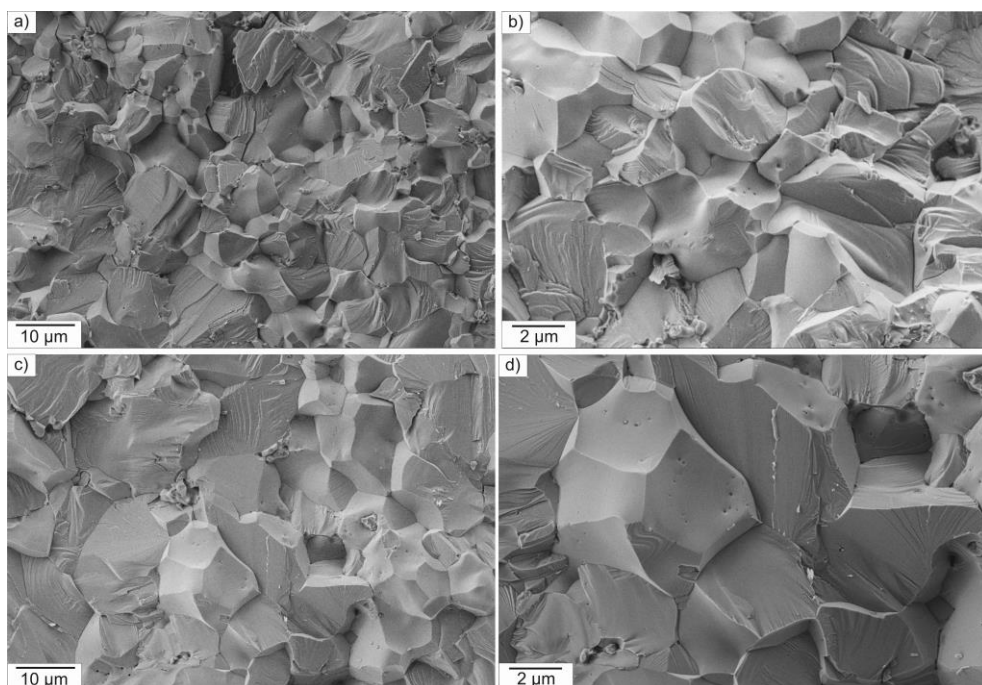

Fig. 4. SEM images of the fracture surfaces: a, b) System I sintered for 5 minutes, c, d) System III sintered for 20 minutes.

CONCLUSIONS

Bulk single-phase (Hf-Ta-Zr-Nb-Ti)C high-entropy carbides were prepared using ball milling and a two-step SPS process.
The main obtained results are:

1. The (Hf-Ta-Zr-Nb-Ti)C high-entropy carbides were prepared with high relative density varying from 99.5 to 99.9 %. The chemical compositions of grains are homogeneous and their average size is in a range of 8 to 11 μm.

2. The influence of the sintering time and indentation load on measured hardness values was found to be not significant. The standard HV1 Vickers hardness values change from 20.2 to 22.0 GPa with the highest value for the system with the largest grain size. This is could be ascribed to the lowest porosity in the system.

3. The values of fracture toughness are in the range of 2.78 MPa to 3.48 MPa, with the highest value for the system with the highest grain size and most dominant toughening mechanisms.

4. The highest bending strength of 284 MPa was measured for the system with the lowest grain size, sintered at the shortest sintering time, with smaller fracture origins in the form of connected grain boundary pores/cracks.

ACKNOWLEDGMENT

REFERENCES
[1] Miracle, DB., Senkov, ON.: Acta Mater., vol. 122, 2017, p. 448–511.
[2] Xiang, H., Xing, Y., Dai, Fz. et al.: Adv. Ceram., vol. 10, 2021, p. 385-441.
[3] Zhang, RZ., Reece, MJ.: J. Mater. Chem. A, vol. 7, 2019, p. 22148–22162.
[4] Oses, C., Toher, C., Curtarolo, S.: Rev. Mater., vol. 5, 2020, p. 295–309.
[5] Castle, E., Csanádi, T., Grasso, S., Dusza, J., Reece, M.: Sci. Rep., vol. 8, 2018, p. 1–12.
[6] Csanádi, T., Vojtko, M., Dankházi, Z., Reece, MJ., Dusza, J.: J. Eur. Ceram. Soc., vol. 40, 2020, p. 4774–4782.
[7] Han, X., Girman, V., Sedlak, R., Dusza, J., Castle, EG., Wang, Y., Reece, M., Zhang, C.: J. Eur. Ceram. Soc., vol. 40, 2020, p. 2709–2715.
[8] Yan, X. et al.: J. Am. Ceram. Soc., vol. 101, 2018, p. 4486–4491.
[9] Feng, L., Fahrenholtz, WG., Hilmas, GE.: J. Am. Ceram. Soc., vol. 102, 2019, p. 7217–7224.
[10] Moskovskikh, DO., Vorotilo, S., Sedegov, AS., Kuskov, KV., Bardasova, KV., Kiryukhantsev-Korneev, PV., Zhukovskyi, M., Mukasyan, AS.: Ceram. Int., vol. 46, 2020, p. 19008–19014.
[11] Dusza, J., Csanádi, T., Medveď, D., Sedlák, R., Vojtko, M., Ivor, M., Ünsal, H., Tatarko, P., Tatarková, M., Šajgalík, P.: J. Eur. Ceram. Soc., vol. 41, 2021, p. 5417–5426.
[12] Anstis, GR., Chantikul, P., Lawn BR., Marshall, DB.: J. Am. Ceram. Soc., vol. 46, 1981, p. 533-538.
[13] ASTM C1161-13 Standard Test Method for Flexural Strength of Advanced Ceramics at Ambient Temperature, (2013) 19.

ANNOUNCEMENTS

Eva Dudrová – 80 years

In November 2021, Assoc. Prof. Ing. Eva Dudrová, PhD. celebrates a significant life event – her 80th birthday.

A native of Nitra, she graduated from the Faculty of Metallurgy of the Technical University in Košice in 1963. After graduating from university, she began a postgraduate course under the supervisions of prof. Jaroslav Kubelík in the field of Physical Metallurgy, where she specialized on powder metallurgy technologies. The workplace was then called the Laboratory of Engineering and Metallurgical Technologies of the Technical University of Košice. Since 1970, this department has become part of the Slovak Academy of Sciences as the Institute of Experimental Metallurgy (now the Institute of Materials Research). In 1969 she passed her final examinations and obtained the degree of "Candidate of Science", and in 1995 she became an associate professor. She worked at IMR SAS as a senior researcher until her retirement in 2015. Throughout her working life, she remained faithful to the field of powder metallurgy.

Assoc. Prof. Eva Dudrová is one of the most important Slovak and European experts in the field of ferrous powder metallurgy with the focus on the powder compaction, sintering, mechanical properties, and fracture miromechanims of sintered steels. She worked as the head of the Department of Ferrous Powder Metallurgy. She was invited to be a member of the research teams in several international projects. Eva Dudrová highly appreciated the Höganäs Chair research projects, which brought together researchers, industrial professionals, and students from more than five countries. She had a wide bilateral collaboration with universities, research institutes, and industry companies practically all over Europe (Vienna University of Technology, Polytechnic of Torino, the company Höganäs AB and others). She was a member of the Editorial Boards of the journals Powder Metallurgy Progress and Metallic Materials. She is the author or co-author of three books, has written more than 200 publications, presented numerous contributions at conferences, organized International Conferences on Powder Metallurgy, Fractography and PM Summer School. Her works have recorded more than 1000 citations. She has trained 8 PhD students. Many of them have become prominent professionals working at universities and in industry in Slovakia and abroad.

The results of her research have also been applied in industry, e.g., in several modifications of technology in powder metallurgy production in Dolný Kubín.

In the competition Scientist of the Year of the Slovak Republic, she was awarded the Honorable Mention for 2008. She was awarded for life-work in basic and applied research in the field of powder metallurgy, for effective contribution to the education of young researchers, pedagogical activity and significant contribution in international cooperation. Through her many years of work, she has contributed to the positive visibility and building of the workplace's reputation at European level. The results of the work ranked her among the recognized experts in the field of basic and applied research

Dear Dr. Eva Dudrová, we all are grateful for your contributions to the science of Powder Metallurgy. On the occasion of your 80th birthday, on behalf of your former colleagues, students and friends, we wish you good health, satisfaction and joy in the family circle.

Miriam Kupková, Pavol Hvizdoš

POWDER METALLURGY PROGRESS,

an international open-access journal with 20 years of publishing history announces the

EXTENSION OF THE JOURNAL`S SCOPE

Works from the fields of powder metallurgy, all powder-derived materials - metals, alloys, ceramics, and composites, basic and applied research of materials science related to mechanical and functional properties, manufacturing, and characterization are always welcomed.

But in 2021 the Scope of the Powder Metallurgy Progress was extended to:

- materials research such as materials physics, materials chemistry, materials engineering, traditional and advanced powder metallurgy, materials processing;
- wide range of metal, ceramic and composite materials including metal matrix, ceramic matrix, polymer matrix composites, and hybrid organic-inorganic-metal-ceramic material systems, structural materials, functional materials, biomaterials, porous materials, magnetic electric and multifunctional materials such as magnetic composites, magnetoelectric, magnetocaloric, ferroelectric, piezoelectric, thermoelectric, magneto-optic, magnetostrictive, or high-temperature materials;
- advanced as well as traditional production technology and processing, additive manufacturing, 3D printing, Press and Sinter, HIP, MIM, PIM, Spark Plasma Sintering, Hot Pressing, Microwave Sintering, Plasma Treatment, Slip Casting, Rapid Heating, Ultrafast Sintering, new progressive compaction and processing methods;
- influence of material processing parameters on their microstructure formation and development and structural relations of physical, mechanical, and functional properties of materials focusing but not limited on powder materials;
- special technological processes of PM material with individual-particular-special physical-chemical properties;
- environmental issues of production and application of PM materials;
- industrial processes, management, and quality, (creation of normative) standard method activity, economical analysis, conception (philosophy)

and prediction in PM and progressive material processing field;
● production of technological equipment for powder and advanced
materials technology.

For more details visit the PMP homepage.

Call for PAPERS!

POWDER METALLURGY PROGRESS

**AN INTERNATIONAL OPEN-ACCESS JOURNAL
WITH 20 YEARS OF PUBLISHING HISTORY
INVITES YOU TO SUBMIT MANUSCRIPTS FOR CONSIDERATION IN THE
FORTHCOMING ISSUE OF THE JOURNAL.**

PUBLISHED BY SCIENDO

Find us on
Facebook/PMPROGRESS